arXiv:1610.04642v1 [cond-mat.mes-hall] 11 Oct 2016

Impurities in a Chern insulator

Vibhuti Bhushan Jha*,[1,2] Garima Rani*,[1,3] and R. Ganesh[1,3]

[1] *The Institute of Mathematical Sciences, C I T Campus, Chennai 600 113, India*
[2] *Indian Institute of Space Science and Technology, Valiamala Road, Valiamala, Thiruvananthapuram, Kerala 695547, India*
[3] *Homi Bhabha National Institute, Training School Complex, Anushakti Nagar, Mumbai 400094, India*

(Dated: October 18, 2016)

Chern insulators arguably provide the simplest examples of topological phases. They are characterized by a topological invariant and can be identified by the presence of protected edge states. In this letter, we show that a local impurity in a Chern insulator induces a twofold response: bound states that carry a chiral current and a net current circulating around the impurity. This is a manifestation of broken time reversal symmetry and persists even for an infinitesimal impurity potential. To illustrate this, we consider a Coulomb impurity in the Haldane model. Working in the low-energy long-wavelength limit, we show that an infinitesimal impurity suffices to create bound states. We find analytic wavefunctions for the bound states and show that they carry a circulating current. In contrast, in the case of a trivial analogue – graphene with a gap induced by a sublattice potential –bound states occur but carry no current. In the many body problem of the Haldane model at half-filling, we use a linear response approach to demonstrate a circulating current around the impurity. In all cases, our results compare well with numerical tight-binding results.

PACS numbers: 71.55.-i,73.20.Hb

Introduction: Chern insulators are lattice analogues of the integer quantum Hall effect in which hopping terms break time reversal symmetry and mimic an external magnetic field. The first Chern insulator was proposed by Haldane in 1988[1] and has since proved to be the starting point for the physics of topological insulators. In this letter, we show that impurities serve as a signature of a Chern insulator by seeding a local chiral current.

The classic signature of a Chern insulator is the occurrence of chiral edge states[2–4]. Our main result – impurity-induced chiral current – can be thought of as a limiting case of an edge current around a hole cut into the sample. Its closed edge will carry edge states and a chiral current. As the hole is shrunk to a point, we are left with a localized impurity potential. The chiral edge current maps to a current that circles the impurity. Furthermore, edge states at the edge of the hole reduce to bound states centred around the impurity. Due to coupling between counter-propagating modes, the bound state energies become discrete and no longer span the gap. Nevertheless, they carry a chiral current. We demonstrate this in the Haldane model with a Coulomb impurity potential, chosen for ease of analytic calculations.

Several studies have focussed on Coulomb impurities in Dirac systems, largely motivated by graphene[5–9]. Here, we focus on gapped Dirac Hamiltonians[10–13]. An insulating gap in graphene can be opened in two ways: (a) by a sublattice potential[14, 15], henceforth referred to as the 'trivial' case, and (b) by a complex next-nearest neighbour hopping – henceforth, the 'non-trivial' case.

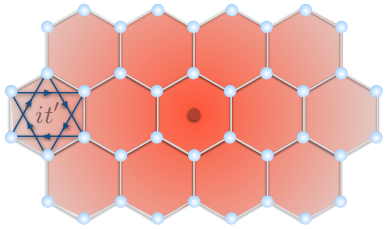

FIG. 1: Honeycomb lattice with a Coulomb impurity. The complex nearest-neighbour hopping of the Haldane model is shown in one plaquette.

While the former breaks inversion symmetry, the latter breaks time reversal symmetry and leads to a Chern insulator – the celebrated Haldane model. In this letter, we perform all calculations for both cases and show that chiral currents only emerge in the non-trivial case.

Coulomb impurity in the Haldane model: We study spinless fermions on a honeycomb lattice described by the Hamiltonian

$$H = -t\sum_{\langle ij\rangle}\{c_i^\dagger c_j + h.c.\} + H_{mass} + \sum_i \frac{g}{|\mathbf{r_i}-\mathbf{r}_0|}c_i^\dagger c_i. \quad (1)$$

The first term represents nearest neighbour hopping as in graphene. The last term represents a repulsive Coulomb impurity located at the centre of one hexagon as shown in Fig 1. The term in the middle represents a mass term, which may be of two types

$$H_{mass,trival} = \sum_{i\in A} V c_i^\dagger c_i - \sum_{i\in B} V c_i^\dagger c_i, \quad (2)$$

$$H_{mass,non-trivial} = it'\sum_{\langle\langle ij\rangle\rangle}\{c_i^\dagger c_j - h.c.\}. \quad (3)$$

*These authors contributed equally to this work.

The numerical results presented below are obtained from the diagonalization of this Hamiltonian on clusters with periodic boundary conditions with the appropriate mass term implemented as above.

In the absence of impurities, this Hamiltonian leads to two Dirac cones at the **K**-points of the Brillouin zone. The mass terms open direct band gaps leading to a semiconductor-like band structure. The long-wavelength response to an impurity is then determined by states near the two **K** points, described by the Hamiltonians[5]

$$\mathcal{H}_{\mathbf{K}} = \begin{pmatrix} -\lambda_{\mathbf{K}} + g/r & \alpha e^{-i\theta}(\partial_r - \frac{i}{r}\partial_\theta) \\ -\alpha e^{i\theta}(\partial_r + \frac{i}{r}\partial_\theta) & \lambda_{\mathbf{K}} + g/r \end{pmatrix},$$
$$\mathcal{H}_{\mathbf{K}'} = \begin{pmatrix} -\lambda_{\mathbf{K}'} + g/r & \alpha e^{i\theta}(\partial_r + \frac{i}{r}\partial_\theta) \\ -\alpha e^{-i\theta}(\partial_r - \frac{i}{r}\partial_\theta) & \lambda_{\mathbf{K}'} + g/r \end{pmatrix}. \quad (4)$$

Due to the rotational symmetry of the impurity potential, we have expressed the Hamiltonian in polar coordinates. In the trivial case, the mass terms are equal, i.e., $\lambda_{\mathbf{K}} = \lambda_{\mathbf{K}'} = V$. In the non-trivial case, we have $\lambda_{\mathbf{K}} = -\lambda_{\mathbf{K}'} = 3\sqrt{3}t'$. We assume that the Coulomb potential does not couple the two valleys; as it decays as $1/q$ in momentum space, scattering with large momentum transfer is suppressed.

Bound states from a single valley: The Coulomb impurity problem for a single valley is well studied[7] (see Supplementary Materials for explicit derivation). The valley Hamiltonians do not commute with angular momentum, $\hat{l}_z = i\hbar\partial_\theta$, but with $\hat{j}_z = \hat{l}_z + \frac{1}{2}\sigma_z$. The eigenstates are characterized by a quantum number $j = m + 1/2$, where m is an integer. The eigenstates in each valley take the form

$$\Psi_{\mathbf{K},j} = \begin{pmatrix} a(r)e^{im\theta} \\ b(r)e^{i(m+1)\theta} \end{pmatrix}, \Phi_{\mathbf{K}',j} = \begin{pmatrix} c(r)e^{-im\theta} \\ d(r)e^{-i(m+1)\theta} \end{pmatrix}, \quad (5)$$

where the radial wavefunctions $a(r) - d(r)$ are related to the radial part of the Hydrogen atom wavefunction. They are linear combinations of terms of the form $r^\chi e^{-r/a_0}\,{}_1\mathcal{F}_1(r)$, where ${}_1\mathcal{F}_1(r)$ is a confluent hypergeometric function. These represent impurity bound states with 'Bohr radius' $a_0 \sim \alpha/\sqrt{\lambda^2_{\mathbf{K}/\mathbf{K}'} - \epsilon^2}$, where ϵ is the energy eigenvalue which is itself determined by j, $|\lambda_{\mathbf{K}/\mathbf{K}'}|$ and the Fermi velocity α.

The eigenstates become unstable beyond a 'supercritical' value of g, in analogy with the Hydrogen atom at $Z = 137$[5, 11, 16–18]. Beyond this instability, well-defined eigenstates may be obtained by regularizing the potential[10]. Indeed, our tight binding spectrum is well-defined for any g due to implicit regularization at the scale of the lattice. As we are mainly concerned with chiral currents in Chern insulators, we always work in the subcritical regime in the interest of simplicity.

Inter-valley mixing: At low energies, the Hamiltonian separates into the two valley-Hamiltonians, $\mathcal{H}_{\mathbf{K}}$ and $\mathcal{H}_{\mathbf{K}'}$. A full eigenstate is a linear combination,

$$\psi_j(\mathbf{r}) \sim \mathcal{A}\Psi_{\mathbf{K},j}e^{i\mathbf{K}.\mathbf{r}} + \mathcal{B}\Phi_{\mathbf{K}',j}e^{-i\mathbf{K}.\mathbf{r}}, \quad (6)$$

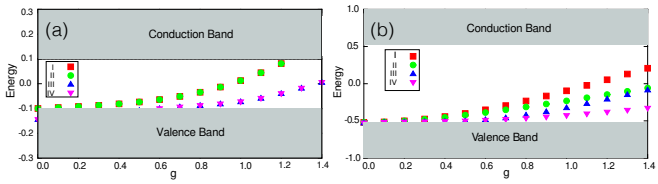

FIG. 2: Bound state spectrum as a function of impurity strength for (a) trivial and (b) non-trivial gaps. The shaded regions represent conduction and valence bands. We have set $V/t = 0.1$ for the trivial case and $t'/t = 0.1$ for the non-trivial case throughout. The tight binding calculation was done on a lattice of 7200 sites.

where $\Psi_{\mathbf{K},j}$ and $\Phi_{\mathbf{K}',j}$ are eigenstates of $\mathcal{H}_{\mathbf{K}}$ and $\mathcal{H}_{\mathbf{K}'}$. The exponential factors $e^{i\mathbf{K}.\mathbf{r}}$ and $e^{-i\mathbf{K}.\mathbf{r}}$ arise as each valley has average momentum $\mathbf{K}$ or $-\mathbf{K}$. We have combined solutions with the same j from both valleys as $\Psi_{\mathbf{K},j}$ and $\Phi_{\mathbf{K}',j}$ are degenerate at the single valley level. The Coulomb impurity allows for weak inter-valley coupling; to lowest order, it will only mix degenerate states which have the same j.

In the trivial case, both valleys have the same mass term. Consequently, $\Psi_{\mathbf{K},j}e^{i\mathbf{K}.\mathbf{r}}$ and $\Phi_{\mathbf{K}',j}e^{-i\mathbf{K}.\mathbf{r}}$ are time-reversed pairs. The valley degree of freedom acts as a pseudospin, allowing us to use Kramer's theorem. As the inter-valley coupling is time-reversal symmetric, the eigenstates remain doubly degenerate as seen from the tight binding spectrum in Fig. 2(a). In contrast, in the non-trivial case shown in Fig. 2(b), the eigenvalues are no longer degenerate.

Comparison with tight binding results: To compare analytic wavefunctions with tight binding results, we compute the probability density of a bound state. In the non-trivial case where we have non-degenerate eigenstates, we find that a symmetric linear combination with $\mathcal{A} = \mathcal{B}$ in Eq. 6 compares well with the highest bound state obtained numerically. Using $\rho = \psi_j^\dagger\psi_j$ with $j = 1/2$ (corresponding to the highest energy eigenvalue), we find (see Supplementary Materials)

$$\rho(r,\theta) = F^2(r)\left[4\lambda_{\mathbf{K}} + \frac{2\alpha}{a_0}\left\{\cos\left(2\mathbf{K}\cdot\mathbf{r}\right) + \cos\left(2\mathbf{K}\cdot\mathbf{r} - 2\theta\right)\right\}\right], \quad (7)$$

where $F(r) = {}_1\mathcal{F}_1(0, 1+2\eta; \frac{2r}{a_0})e^{-\frac{r}{a_0}}r^{\eta-\frac{1}{2}}\mathcal{N}$, with $\eta = \sqrt{\frac{1}{4} - \frac{g^2}{\alpha^2}}$ and $\mathcal{N}$ being a normalisation constant.

Fig. 3(top) shows the tight binding results (blue dots) for ρ vs. r, distance from impurity. Comparing this with the analytical result presents two difficulties: (a) we do not have a closed form expression for the constant of normalization $\mathcal{N}$, (b) the analytic wavefunction is 'coarse-grained', i.e., it gives us a continuous function for density. To connect to the numerical result, we must integrate this result over an effective area corresponding to each lattice point. Once again, this does not give us a closed analytic form. To account for these two fac-

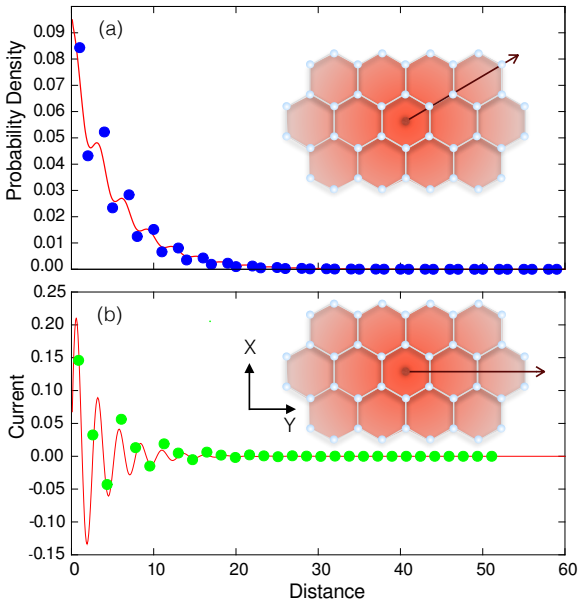

FIG. 3: Wavefunction of highest energy bound state for $g = 0.2$. (a) Probability density vs. distance from impurity at points along the line shown in inset. (b) Current vs. distance. Current is evaluated on bonds along the line indicated. Red lines show analytical result with an overall multiplicative fitting parameter (= 10). Dots are tight binding results.

tors, we introduce a single fitting parameter – an overall multiplicative constant. We then obtain excellent agreement between the analytic result and the tight binding calculations as shown in Fig. 3.

Current in the bound state: In the trivial case, bound states cannot carry current due to time reversal symmetry. In the non-trivial case, we find that bound states carry a chiral current encircling the impurity. This is shown in Fig. 3 with analytical and numerical results for the highest bound state for $g = 0.2$. The analytic result is computed as the expectation value of the bond current operator in the wavefunction of Eq. 6 with $\mathcal{A} = \mathcal{B}$ (see Supplementary Materials). As with the probability density, we obtain good agreement using just one multiplicative fitting parameter.

As shown in Fig. 4, the bound state current circulates along loops surrounding the impurity. We focus on nearest-neighbour bonds as next-nearest neighbours carry a complex hopping term that induces a current even without an impurity. Typically, we find that the highest bound state has strongest current along the hexagon immediately surrounding the impurity, see Fig. 4(a). In lower bound states, the current strength may peak further away from the impurity. The current direction may also change with increasing loop radius, see Fig. 4(b).

Total current from linear response: Apart from individual bound states, tight binding calculations at half-filling show a total chiral current encircling the impurity in the non-trivial case, as shown in Fig. 5(a). We describe

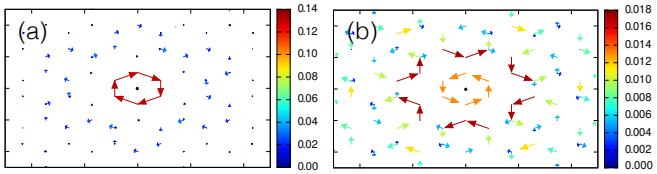

FIG. 4: Tight binding results for current carried by bound states. (a) Current in the highest bound state for g = 0.72. (b) Current in the second highest bound state for g = 0.3. The color and length of an arrow show the amplitude of current on that particular bond; current direction is indicated by the arrow head. The color bar gives the current in units of t, the nearest neighbour hopping.

this using a linear response approach.

In the clean Haldane model, the Green's function is

$$\mathcal{G}^0_{\gamma,\delta}(\mathbf{k},\omega) = \langle \bar{\psi}_{\mathbf{k},\omega,\gamma}\psi_{\mathbf{q},\omega,\delta}\rangle = \sum_{l=\pm1} \frac{\mathcal{T}_{\gamma l}\mathcal{T}^{\dagger}{}_{l\delta}}{i\omega - \epsilon_{k,l}}. \quad (8)$$

Here, ψ's are Grassmann numbers, $\gamma, \delta = A/B$ are sublattice indices, and $\omega = (2m+1)\pi k_B T$ is a fermionic Matsubara frequency. The matrix $\mathcal{T}$ diagonalizes the 2×2 Hamiltonian matrix, giving eigenvalues $\epsilon_{k,l}$. It may be written as

$$\mathcal{T} = \begin{pmatrix} \cos(\frac{\theta_{\mathbf{k}}}{2}) & -e^{-i\phi_{\mathbf{k}}}\sin(\frac{\theta_{\mathbf{k}}}{2}) \\ e^{i\phi_{\mathbf{k}}}\sin(\frac{\theta_{\mathbf{k}}}{2}) & \cos(\frac{\theta_{\mathbf{k}}}{2}) \end{pmatrix}. \quad (9)$$

Near the two Dirac points at $\pm\mathbf{K}$, the parameters $\theta_{\mathbf{k}}$ and $\phi_{\mathbf{k}}$ take simple forms, given by $\cos(\theta_{\mathbf{k}}) = \frac{\mp\lambda_{\mathbf{K}}}{\sqrt{k_x^2+k_y^2+\lambda_{\mathbf{K}}^2}}$ and $e^{i\phi_{\mathbf{k}}} = \frac{\pm k_y - ik_x}{\sqrt{k_x^2+k_y^2}}$. We have set the chemical potential to zero as we are at half-filling.

Taking the impurity potential to be small, $g \ll \lambda_{\mathbf{K}}, \lambda_{\mathbf{K}'}$, the perturbation term in the action is given by

$$S_1 = \frac{2\pi g}{N}\sum_{\mathbf{k},\mathbf{q},\omega}\frac{1}{q}\left[\bar{\psi}_{\mathbf{k},\omega,A}\psi_{\mathbf{k}+\mathbf{q},\omega,A} + \bar{\psi}_{\mathbf{k},\omega,B}\psi_{\mathbf{k}+\mathbf{q},\omega,B}\right], \quad (10)$$

obtained by Fourier transforming the Coulomb impurity potential. We are interested in the current on a given bond connecting $(i, A) \to (j, B)$, given by the operator

$$\mathcal{J}^{j,B}_{i,A} = it(\bar{\psi}_{i,A,\tau}\psi_{j,B,\tau} - \bar{\psi}_{j,B,\tau}\psi_{i,A,\tau}). \quad (11)$$

Using standard linear response theory,

$$\langle \mathcal{J}^{j,B}_{i,A}\rangle - \langle \mathcal{J}^{j,B}_{i,A}\rangle_0 = \langle \mathcal{J}^{j,B}_{i,A}\rangle_0\langle S_1\rangle_0 - \langle S_1\mathcal{J}^{j,B}_{i,A}\rangle_0. \quad (12)$$

The notation $\langle\{.\}\rangle_0$ denotes expectation value with respect to the unperturbed action. The second term on the left hand side vanishes as current is zero for inter-sublattice bonds in the clean limit. The right hand side can be evaluated using Wick's theorem to give

$$\langle \mathcal{J}^{j,B}_{i,A}\rangle = \frac{it}{N^2\beta}\sum_{\mathbf{k},\mathbf{q},\omega,\kappa}\frac{2\pi g}{q}\left[\mathcal{G}^0_{B,\kappa}(\mathbf{k},\omega)\mathcal{G}^0_{\kappa,A}(\mathbf{k}+\mathbf{q},\omega)e^{-i\theta_1} - \mathcal{G}^0_{A,\kappa}(\mathbf{k},\omega)\mathcal{G}^0_{\kappa,B}(\mathbf{k}+\mathbf{q},\omega)e^{-i\theta_2}\right], \quad (13)$$

where, $\theta_1 = \mathbf{k}\cdot\mathbf{r_j} - (\mathbf{k}+\mathbf{q})\cdot\mathbf{r_i}$ and $\theta_2 = \mathbf{k}\cdot\mathbf{r_i} - (\mathbf{k}+\mathbf{q})\cdot\mathbf{r_j}$. The index κ sums over sublattices A and B, while N is the number of sites in the system. We obtain

$$\langle \mathcal{J}^{j,B}_{i,A} \rangle = k_B T \sum_{\mathbf{k},\mathbf{q},\omega,\kappa,l,l'} \frac{F_{ll',\kappa}}{(i\omega - \epsilon_{\mathbf{k},l})(i\omega - \epsilon_{\mathbf{k}+\mathbf{q},l'})}, \quad (14)$$

where $F_{ll',\kappa}$ is given by

$$F_{ll',\kappa} = it\frac{2\pi g}{N^2 q}\Big[\mathcal{T}_{\kappa l}(\mathbf{k}+\mathbf{q})\mathcal{T}^{\dagger}_{lA}(\mathbf{k}+\mathbf{q})\mathcal{T}_{Bl'}(\mathbf{k})\mathcal{T}^{\dagger}_{l'\kappa}(\mathbf{k})e^{-i\theta_1} - \mathcal{T}_{Al}(\mathbf{k})\mathcal{T}^{\dagger}_{l\kappa}(\mathbf{k})\mathcal{T}_{\kappa l'}(\mathbf{k}+\mathbf{q})\mathcal{T}^{\dagger}_{l'B}(\mathbf{k}+\mathbf{q})e^{-i\theta_2}\Big]. \quad (15)$$

In the momentum sums in Eq. 14, we only keep intra-valley terms, i.e., $\mathbf{k}$ and $\mathbf{k}+\mathbf{q}$ are taken to be in the same valley. This is justified due to the factor of $\frac{1}{q}$ in Eq. 15, which in turn comes from the Fourier transform of the Coulomb potential. This strongly suppresses inter-valley terms which require a large q.

To better understand the current distribution, we denote the bond as $(\mathbf{R},\delta)$, where $\mathbf{R}$ is the distance of the impurity from the centre of the bond and δ is the bond vector. After summing over Matsubara frequencies, assuming zero temperature, we obtain the bond current

$$\langle \mathcal{J}^{j,B}_{i,A} \rangle = \frac{t}{N^2}\sum_{\mathbf{k},\mathbf{q}} \frac{4\pi g \lambda_{\mathbf{K}} \cos(\mathbf{k}\cdot\delta)\cos(\frac{\mathbf{q}}{2}\cdot\delta)}{q(-\zeta_{\mathbf{k}} - \zeta_{\mathbf{k}+\mathbf{q}})\zeta_{\mathbf{k}+\mathbf{q}}\zeta_{\mathbf{k}}} \times \{q_x \sin(\mathbf{K}\cdot\delta) + q_y\cos(\mathbf{K}\cdot\delta)\}\sin(\mathbf{q}\cdot\mathbf{R}), \quad (16)$$

where $\zeta_{\mathbf{k}} = \sqrt{k_x^2 + k_y^2 + \lambda^2_{\mathbf{K}}}$ is the absolute value of the excitation energies at $\mathbf{k}$. We notice that the current depends on $\mathbf{R}$ solely through the $\sin(\mathbf{q}\cdot\mathbf{R})$ term above. Far from the impurity, when $|\mathbf{R}| \gg a$ (the lattice spacing), this term will be highly oscillatory. Therefore, the dominant terms in the above summation will come from small $\mathbf{q}$ values. Taking $\mathbf{R}$ along y and δ along x direction (see Fig. 3(b)), we rewrite the summation as an integral,

$$\langle \mathcal{J}^{j,B}_{i,A} \rangle \sim \int dq_y q_y \sin(q_y R). \quad (17)$$

We have kept only the leading order term in q_y as the summation is dominated by small q_y values. The integral scales as q_y^2. As R is the only distance scale, the bond current will scale as $1/R^2$ for large R. Indeed, this is confirmed by our tight binding analysis. Fig. 5(b) shows the current as a function of R for $g = 0.5$. For large R, we obtain a good fit to the form $J = aR^{-b}$, with the exponent $b \approx 2$. Thus, remarkably, the total bond current induced by the impurity decays algebraically as R^{-2} in contrast to the exponentially decaying bound state currents. We surmise that the dominant contribution to currents comes from extended states of the valence band, rather than from bound states.

While linear response is justified for small g, we numerically see that the current scales linearly with g over a large window, as shown in Fig. 5(c). Here, total current is defined as the sum of bond currents on all bonds intersecting the indicated line in Fig. 3(b). Surprisingly, deviation from linearity sets in at $g \sim 1.15$ which is the 'supercritical' threshold at which the energy of the highest bound state becomes zero[10], see Fig. 2(b).

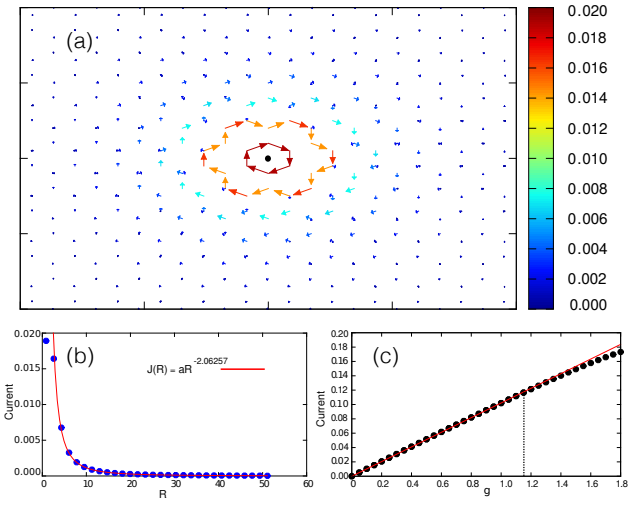

FIG. 5: Tight binding results for total current around impurity. (a) Currents on bonds near impurity (g=0.5); the sites surrounding the impurity organize themselves into loops. (b) Current vs. distance from impurity for g = 0.5. For large distances, $J(R) \sim 1/R^2$, in agreement with the linear response result. (c) Total current vs. g. The current is linear upto g $\sim$ 1.15, indicating a wide window of validity of our linear response result.

Discussion: We have shown that impurities in a Chern insulator induce chiral currents, providing a signature of the underlying topology. This builds upon earlier work on the effect of impurities on Hall currents[19] and the existence of bound states in topological phases[20, 21]. While we have explicitly shown results for Coulomb impurities above, we find that any impurity potential induces a chiral current. Our results could be tested with the recent cold atom realization of the Haldane model[22] and with graphene-like candidate materials[23].

Our results also have implications for time reversal symmetric weak topological insulators which can be thought of as two copies of a Chern insulator, one for each spin[24]. An impurity will induce chiral currents of opposite directions in each spin sector leading to a chiral spin current rather than a charge current. Similar features may also occur in other topological systems.

Chiral currents will also occur in non-graphene-like systems, most interestingly in time-reversal broken chiral superconductivity, e.g., in $SrRu_2O_4$[25]. Edge states in $SrRu_2O_4$ have evaded detection as they are composed of electrons and hole components which counteract, leading to a weak edge charge current[26]. Unlike an edge, a repulsive impurity induces a preference for hole-like over

electron-like bound states. As a result, impurity-induced chiral currents may be stronger, constituting a clear experimental signature. Impurity induced chiral currents will also serve as signatures for the proposed chiral superconducting phases of graphene[27–29] and $TiSe_2$ [30].

Acknowledgments: We thank Arnab Sen and Kumar S. Gupta for discussions.

[1] F. D. M. Haldane, Phys. Rev. Lett. **61**, 2015 (1988).
[2] B. I. Halperin, Phys. Rev. B **25**, 2185 (1982).
[3] N. Hao, P. Zhang, Z. Wang, W. Zhang, and Y. Wang, Phys. Rev. B **78**, 075438 (2008).
[4] R. S. K. Mong and V. Shivamoggi, Phys. Rev. B **83**, 125109 (2011).
[5] V. M. Pereira, J. Nilsson, and A. H. Castro Neto, Phys. Rev. Lett. **99**, 166802 (2007).
[6] R. R. Biswas, S. Sachdev, and D. T. Son, Phys. Rev. B **76**, 205122 (2007).
[7] D. S. Novikov, Phys. Rev. B **76**, 245435 (2007).
[8] I. S. Terekhov, A. I. Milstein, V. N. Kotov, and O. P. Sushkov, Phys. Rev. Lett. **100**, 076803 (2008).
[9] S. K. Gupta, A. Samsarov, and S. Sen, The European Physical Journal B **73**, 389 (2010).
[10] V. M. Pereira, V. N. Kotov, and A. H. Castro Neto, Phys. Rev. B **78**, 085101 (2008).
[11] K. S. Gupta and S. Sen, Phys. Rev. B **78**, 205429 (2008).
[12] W. Zhu, Z. Wang, Q. Shi, K. Y. Szeto, J. Chen, and J. G. Hou, Phys. Rev. B **79**, 155430 (2009).
[13] B. Skinner, B. I. Shklovskii, and M. B. Voloshin, Phys. Rev. B **89**, 041405 (2014).
[14] G. W. Semenoff, Phys. Rev. Lett. **53**, 2449 (1984).
[15] B. Hunt, J. D. Sanchez-Yamagishi, A. F. Young, M. Yankowitz, B. J. LeRoy, K. Watanabe, T. Taniguchi, P. Moon, M. Koshino, P. Jarillo-Herrero, and R. C. Ashoori, Science **340**, 1427 (2013).
[16] V. Berestetskii, E. Lifshitz, and L. Pitaevskii, *Quantum Electrodynamics (Second Edition)* (Butterworth-Heinemann, Oxford, 1982) pp. xiii – xv.
[17] K. S. Gupta and S. Sen, Modern Physics Letters A **24**, 99 (2009).
[18] O. V. Gamayun, E. V. Gorbar, and V. P. Gusyunin, Ukr. J. Phys. **56**, 688 (2011).
[19] R. E. Prange, Phys. Rev. B **23**, 4802 (1981).
[20] R.-J. Slager, L. Rademaker, J. Zaanen, and L. Balents, Phys. Rev. B **92**, 085126 (2015).
[21] L. Kimme and T. Hyart, Phys. Rev. B **93**, 035134 (2016).
[22] G. Jotzu, M. Messer, R. Desbuquois, M. Lebrat, T. Uehlinger, D. Greif, and T. Esslinger, Nature (London) **515**, 237 (2014), arXiv:1406.7874 [cond-mat.quant-gas] .
[23] J. Mao, Y. Jiang, D. Moldovan, G. Li, K. Watanabe, T. Taniguchi, M. R. Masir, F. M. Peeters, and E. Y. Andrei, Nat Phys **12**, 545 (2016).
[24] C. L. Kane and E. J. Mele, Phys. Rev. Lett. **95**, 226801 (2005).
[25] C. Kallin and A. J. Berlinsky, Journal of Physics: Condensed Matter **21**, 164210 (2009).
[26] W. Huang, S. Lederer, E. Taylor, and C. Kallin, Phys. Rev. B **91**, 094507 (2015).
[27] S. Pathak, V. B. Shenoy, and G. Baskaran, Phys. Rev. B **81**, 085431 (2010).
[28] R. Nandkishore, L. S. Levitov, and A. V. Chubukov, Nat Phys **8**, 158 (2012).
[29] A. M. Black-Schaffer, Phys. Rev. Lett. **109**, 197001 (2012).
[30] R. Ganesh, G. Baskaran, J. van den Brink, and D. V. Efremov, Phys. Rev. Lett. **113**, 177001 (2014).
[31] S.-H. Dong, Journal of Physics A: Mathematical and General **36**, 4977 (2003).

SUPPLEMENTARY MATERIAL

We follow the derivation of bound state wavefunctions presented in Ref. 7 here, while highlighting the differences between the trivial and non-trivial cases.

Non-Trivial case - solutions from each valley: The Hamiltonians discussed in the main text (Eq. 4) have spinor solutions of the form given in Eq. 5. We discuss this for the **K** valley below; similar arguments apply for the **K′** valley as well. Performing a transformation of the form $a(r)\sqrt{r} = A(r)$ and $b(r)\sqrt{r} = B(r)$, we obtain the differential equations:

$$B'(r) + \frac{j}{r}B(r) = \frac{1}{\alpha}(\epsilon + \lambda_{\mathbf{K}} - \frac{g}{r})A(r),$$
$$A'(r) - \frac{j}{r}A(r) = -\frac{1}{\alpha}(\epsilon - \lambda_{\mathbf{K}} - \frac{g}{r})B(r). \quad \text{(S1)}$$

We are interested in bound states in the gap, $-\lambda_{\mathbf{K}} < \epsilon < \lambda_{\mathbf{K}}$. A coordinate scaling of the form $\rho = 2\mu r$, with $\mu = \sqrt{\lambda_K^2 - \epsilon^2}$, gives

$$B'(\rho) + \frac{j}{\rho}B(\rho) = \left(-\frac{g}{\alpha\rho} + \frac{1}{2\alpha}\sqrt{\frac{\lambda_{\mathbf{K}}+\epsilon}{\lambda_{\mathbf{K}}-\epsilon}}\right)A(\rho),$$
$$A'(\rho) - \frac{j}{\rho}A(\rho) = \left(\frac{g}{\alpha\rho} + \frac{1}{2\alpha}\sqrt{\frac{\lambda_{\mathbf{K}}-\epsilon}{\lambda_{\mathbf{K}}+\epsilon}}\right)B(\rho). \quad \text{(S2)}$$

For notational convenience, we denote $\mu_\pm = \sqrt{\lambda_{\mathbf{K}} \pm \epsilon}$. The above differential equations are coupled and can be separated[7] by taking $B(\rho) = \mu_+(f_1^{\mathbf{K}} - f_2^{\mathbf{K}})$ and $A(\rho) = \mu_-(f_1^{\mathbf{K}} + f_2^{\mathbf{K}})$. Substitution in Eqs. S2 gives

$$f_2'^{\mathbf{K}} + f_2^{\mathbf{K}}(\frac{1}{2\alpha} + \frac{\tau_2}{\alpha\rho}) = f_1^{\mathbf{K}}(\frac{j}{\rho} + \frac{\tau_1}{\alpha\rho}),$$
$$f_1'^{\mathbf{K}} - f_1^{\mathbf{K}}(\frac{1}{2\alpha} + \frac{\tau_2}{\alpha\rho}) = f_2^{\mathbf{K}}(\frac{j}{\rho} - \frac{\tau_1}{\alpha\rho}), \quad \text{(S3)}$$

where $\tau_1 = \frac{g\lambda}{\mu}$ and $\tau_2 = \frac{g\epsilon}{\mu}$. These equations can be decoupled to resemble the general Tricomi equation[31],

$$\frac{d^2 f_{1,2}^{\mathbf{K}}}{d\rho^2} + \frac{1}{\rho}\frac{df_{1,2}^{\mathbf{K}}}{d\rho} + \left(-\frac{1}{4\alpha^2} - \frac{\tau_2 \pm \frac{\alpha}{2}}{\alpha^2\rho} - \frac{\eta^2}{\rho^2}\right)f_{1,2}^{\mathbf{K}} = 0, \quad \text{(S4)}$$

where, $\eta = \sqrt{j^2 - g^2/\alpha^2}$. The solutions of Eq. S4 for $f_1^{\mathbf{K}}(\rho)$ and $f_2^{\mathbf{K}}(\rho)$ are

$$f_1^{\mathbf{K}}(\rho) = {}_1\mathcal{F}_1(1 + \frac{\tau_2}{\alpha} + \eta, 1 + 2\eta, \frac{\rho}{\alpha})e^{-\frac{\rho}{2\alpha} + \eta\log\rho}c_1, \quad \text{(S5)}$$

$$f_2^{\mathbf{K}}(\rho) = {}_1\mathcal{F}_1(\frac{\tau_2}{\alpha} + \eta, 1 + 2\eta, \frac{\rho}{\alpha})e^{-\frac{\rho}{2\alpha} + \eta\log\rho}c_2, \quad \text{(S6)}$$

where, c_1 and c_2 are constants and ${}_1\mathcal{F}_1(a, c; z) = 1 + \frac{az}{c1!} + \frac{a(a+1)z^2}{c(c+1)2!} + \ldots$ is the confluent Hypergeometric function. When a is a non-positive integer, the function ${}_1\mathcal{F}_1$ reduces to a polynomial and becomes square-integrable[16]. We obtain the energy spectrum from this condition by writing $\frac{\tau_2}{\alpha} + \eta = \beta$, where β is a non positive integer.

Similar arguments give us solutions for the **K′** valley, with $C(\rho) = \mu_+(f_1^{\mathbf{K}'} + f_2^{\mathbf{K}'})$ and $D(\rho) = \mu_-(f_1^{\mathbf{K}'} - f_2^{\mathbf{K}'})$, where $c(r)\sqrt{r} = C(r)$ and $d(r)\sqrt{r} = D(r)$. This leads to

$$f_2^{\mathbf{K}'}(\rho) = {}_1\mathcal{F}_1(1 + \frac{\tau_2}{\alpha} + \eta, 1 + 2\eta, \frac{\rho}{\alpha})c_1 e^{-\frac{\rho}{2\alpha} + \eta\log\rho}$$
$$f_1^{\mathbf{K}'}(\rho) = {}_1\mathcal{F}_1(\frac{\tau_2}{\alpha} + \eta, 1 + 2\eta, \frac{\rho}{\alpha})c_2 e^{-\frac{\rho}{2\alpha} + \eta\log\rho} \quad \text{(S7)}$$

Comparing the solutions at the two valleys, we find that $f_1^{\mathbf{K}'}(\rho) = f_2^{K}(\rho)$ and $f_2^{\mathbf{K}'}(\rho) = f_1^{\mathbf{K}}(\rho)$.

Trivial case - solutions from each valley: The solutions for the trivial case again have the the spinor form of Eq. 5. But, the radial part separates out such that the equations are the same for both valleys. It is sufficient to find analytical expressions for the functions $f_1^{\mathbf{K}}$ and $f_2^{\mathbf{K}}$ for the **K** valley. We denote $f_1^{\mathbf{K},\mathbf{K}'} = f_1$ and $f_2^{\mathbf{K},\mathbf{K}'} = f_2$. The radial wavefunctions take the form $A(\rho), C(\rho) = \mu_+(f_1 + f_2)$ and $B(\rho), D(\rho) = \mu_-(f_1 - f_2)$ Following the same procedure as in the non trivial case, we obtain the following differential equations,

$$\frac{d^2 f_{1,2}}{d\rho^2} + \frac{1}{\rho}\frac{df_{1,2}}{d\rho} + \left(-\frac{1}{4\alpha^2} - \frac{\tau_2 \mp \frac{\alpha}{2}}{\alpha^2\rho} - \frac{\eta^2}{\rho^2}\right)f_{1,2} = 0. \quad \text{(S8)}$$

This equation also has solutions which are confluent hypergeometric function similar to Eqs. S7.

Analytical form of wavefunction: The radial wavefunctions $a(r) - d(r)$ in spinors $\Psi_{\mathbf{K}}$ and $\Phi_{\mathbf{K}'}$ (Eq. 5) can be deduced by series of transformations mentioned earlier. The non trivial wavefunctions at **K** and **K′** are given by

$$a(r), c(r) = \mathcal{N}\mu_\mp e^{-\frac{\mu r}{\alpha}} r^{\eta - \frac{1}{2}} \Big({}_1\mathcal{F}_1(1 + \frac{\tau_2}{\alpha} + \eta, 1 + 2\eta; 2\frac{\mu}{\alpha}r)c_1$$
$$+ {}_1\mathcal{F}_1(\eta + \frac{\tau_2}{\alpha}, 1 + 2\eta; 2\frac{\mu}{\alpha}r)c_2\Big),$$

$$b(r), d(r) = \pm\,\mathcal{N}\mu_\pm e^{-\frac{\mu r}{\alpha}} r^{\eta - \frac{1}{2}} \Big({}_1\mathcal{F}_1(1 + \frac{\tau_2}{\alpha} + \eta, 1 + 2\eta; 2\frac{\mu}{\alpha}r)c_1$$
$$- {}_1\mathcal{F}_1(\eta + \frac{\tau_2}{\alpha}, 1 + 2\eta; 2\frac{\mu}{\alpha}r)c_2\Big), \quad \text{(S9)}$$

where, '$\pm$' denotes $+$ for the **K** valley and $-$ for the **K′** valley respectively. c_1 and c_2 are constants, while $\mathcal{N}$ is a normalization constant.

Probability Density from bound state wavefunction: The probability density in terms of the full eigenstate is given by the expression $\rho = \psi_j^\dagger\psi_j$ with $j = 1/2$ – this is the sum of the densities on both sublattices. The wavefunction ψ_j is now a linear combination of eigenstates from each valley. Thus, we substitute the expression from Eq. 5 of the main text in Eq. 6 of the main text to obtain:

$$\rho = a^2 + b^2 + c^2 + d^2 + 2(ac\cos(2\mathbf{K}\cdot\mathbf{r}) + bd\cos(2\mathbf{K}\cdot\mathbf{r} + 2\theta)), \quad \text{(S10)}$$

This is the general expression for the probability density from which we can obtain the probability density for any bound state using the explicit wavefunctions given in Eq. S9. We choose $j = 1/2$ to describe the highest bound state, since $j = 1/2$ corresponds to the highest bound state energy at the single valley level.

The choice of $j = 1/2$ makes the first argument of one of the confluent hypergeometric functions zero, i.e., $\frac{\tau_2}{\alpha} + \eta = 0$. This makes the choice of c_1 irrelevant as one of the confluent hypergeometric functions becomes zero[7],[31]. With this simplification, we obtain Eq. 7 of the main text after absorbing the coefficient c_2 into $\mathcal{N}$.

Current expression for bound state: Proceeding in the same way as discussed in the previous section on density, we can find the current using the bond current expression $\mathcal{J}_{i,A}^{j,B} = it\{\psi_A^*(i)\psi_B(j) - \psi_B^*(j)\psi_A(i)\}$. We reexpress the site positions using δ, the bond vector, and $\mathbf{R}$, the distance of the bond center from the impurity, so that $\mathbf{r}_i = \mathbf{R} - \delta/2$ and $\mathbf{r}_j = \mathbf{R} + \delta/2$. We take $\mathbf{R}$ to be along the horizontal direction and δ to be vertical - see Fig. 3(b) of the main text. We further assume $|\mathbf{R}| \gg \delta$ for simplicity. Using the analytic wavefunctions of Eqs. S9 in Eq. 6 of the main text (we take $\mathcal{A} = \mathcal{B}$), we find the following expression for the bond current,

$$\mathcal{J} = 4tF^2(R)\lambda_{\mathbf{K}} \sin(2|\mathbf{K}|R), \tag{S11}$$

where $F(r)$ is defined in the main text. This expression is plotted as the red curve in Fig. 3(b) of the main text (upto an overall scaling factor).